Phonon replicas at the *M* point in 4*H*-SiC: A theoretical and experimental study

I. G. Ivanov, U. Lindefelt,* A. Henry,* O. Kordina,† and C. Hallin*
Department of Physics and Measurement Technology, Linköping University, S-581 83 Linköping, Sweden

M. Aroyo
Department of Condensed Matter Physics, Sofia University, 1126 Sofia, Bulgaria

T. Egilsson and E. Janzén
Department of Physics and Measurement Technology, Linköping University, S-581 83 Linköping, Sweden
(Received 16 June 1998)

This paper presents a comprehensive study of the phonons at the *M* point of the Brillouin zone of 4*H*-SiC, i.e., at the position of the conduction-band minimum, from both theoretical and experimental points of view. The phonon energies are derived from the low-temperature photoluminescence (PL) spectrum. The theoretical section contains the classification of phonons by symmetry, the deduction of the polarization selection rules for the photons emitted during recombination of free or nitrogen-bound excitons, and presents a simple lattice dynamics model used to obtain some results on the distribution of the phonon modes with different symmetries above and below the energy gap in the phonon dispersion. The classification of the 24 phonons by symmetry is shown to be $8M_1+4M_2+4M_3+8M_4$, where M_i are the irreducible representations of the group of the wave vector at the *M* point. The polarization selection rules imply that among the 24 phonon replicas (lines) in 4*H*-SiC, which can be observed in the PL spectrum, there are 12 with parallel polarization (M_1 and M_3 symmetry), and 12 with polarization perpendicular (M_2 and M_4 symmetry) to the crystal (hexagonal) *c* axis. Our consideration shows that the phonons of each symmetry are equally distributed above and below the ''phonon'' energy gap. Therefore, there are six replicas of each polarization above and below the gap. In the experimental section an assignment of the phonon replicas based on the similarity of the sets of replicas related to the bound and free excitons is carried out, and the results are compared with the theoretical ones. We have experimentally found 22 of the 24 phonons at the *M* point in 4*H*-SiC. [S0163-1829(98)02144-4]

I. INTRODUCTION

SiC is a promising material for future device application, especially in the cases when operation at high power, high temperatures, and/or high radiation levels is required. Nowadays, chemical vapor deposition (CVD)-grown epilayers of high crystalline quality and doping levels as low as 10^{14} cm^{-3} of both 6*H* and 4*H* polytypes are available.[1] 4*H*-SiC is the subject of study in the present paper.

The most common doping impurities in nominally undoped SiC are the nitrogen (N on C site, or N_C) donor and the aluminum (AI_{Si}) acceptor. Sharp lines originating from these impurities are usually seen in the low temperature near-band-gap photoluminescence (PL) spectrum. This technique is nondestructive, and the most informative one among the different techniques for characterization of the grown material. Besides N and Al, many other impurities can also be detected (e.g., H, Ti, Ga;[2–4] for a recent review on the optical characterization of various SiC polytypes, see Ref. 5). In the case of very pure crystals, photon emission due to recombination of free excitons can be observed, and this provides a tool for determination of the nitrogen doping concentration from the PL spectrum.[6,7] Thus a detailed knowledge of the spectrum is of practical importance, because it yields important information used as feedback for further improvement of the CVD growth. The following presentation deals with the structure of the PL spectrum of 4*H*-SiC.

A typical PL spectrum at 2 K of a high-quality CVD-grown 4*H*-SiC epilayer is shown in Fig. 1. The spectrum consists of numerous sharp lines which are identified as zero-phonon lines of the N- and Al-bound excitons, and phonon replicas of the N-bound and free excitons (FE's). The structure of the spectrum is quite well understood at present. However, for the sake of clearness and completeness of presentation, in this introduction we shall consider the origin of

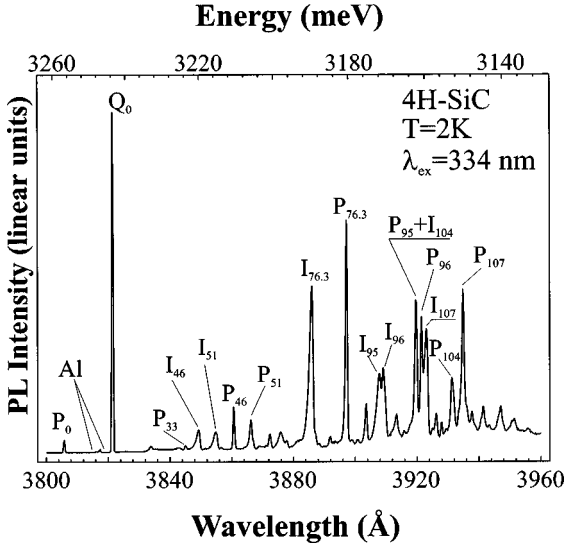

FIG. 1. Typical PL spectrum of unintentionally low doped 4*H*-SiC at $T=2$ K.

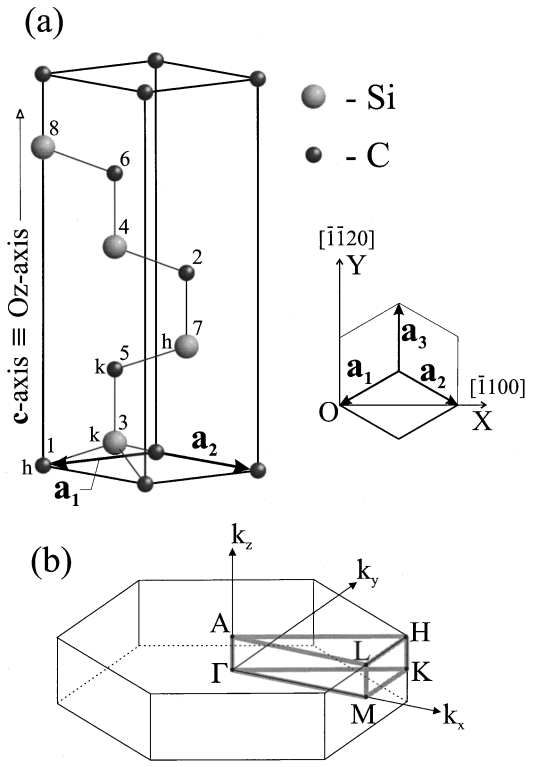

FIG. 2. (a) The unit cell, and (b) the first Brillouin zone of 4*H*-SiC (the irreducible part of the zone is outlined). The inequivalent hexagonal and cubic positions for the C and Si atoms are denoted with *h* and *k* for the hexagonal and cubic sites, respectively. The atoms are enumerated in such a way that the pairs of subsequent numbers (1,2), (3,4), (5,6), and (7,8) denote equivalent atoms, i.e., atoms belonging to one and same orbit. The insert in part (a) of the figure shows the relation between the crystallographic axis Oa_1a_2 and the Cartesian coordinates *Oxy* in the basal plane (the axis *Oz* coincides with the *c* axis).

the different lines in some detail. Within this work we shall concentrate mainly on the sets of PL lines due to the N-bound exciton and the FE's. The structure of acceptor-BE (bound exciton) related lines is different and will not be considered here (see Refs. 4 and 8 for the cases of Al and Ga acceptors).

Similar to all known SiC polytypes, 4*H*-SiC is an indirect band-gap semiconductor. The space group is, using different standard notations C_{6v}^4 (Schoenflies notation), $P6_3mc$ (international notation), or space group number 186 (see, for instance, Refs. 9 and 10). It is a nonsymmorphic space group. According to numerous electronic band-structure calculations,[11] the three equivalent conduction-band minima are located at the point *M* of the Brillouin zone (BZ); see Fig. 2(b). The maximum of the valence band is at the center Γ. Thus, an electron-hole pair coupled in a free exciton has a crystal momentum $\mathbf{k}_M$, where $\mathbf{k}_M$ is the momentum corresponding to the *M* point of the BZ. Consequently, direct recombination of the electron and the hole is forbidden because of the crystal-momentum conservation law. To conserve the crystal momentum the FE recombination is only possible with the assistance of another particle (or quasiparticle). In an ideal crystal, the role of such a particle is played by a phonon. In a real crystal with defects the excitons can bind to them. Let us consider, for instance, the donor impurity N, replacing a C atom at one of the two inequivalent sites in 4*H*-SiC, hexagonal or cubic [denoted in Fig. 2(a) *h* and *k*, respectively]. The recombination of a nitrogen-bound exciton (N-BE) is possible either in a process when the impurity atom takes the momentum itself, or in a phonon-assisted process. The former process gives rise to the so-called zero-phonon line (P_0 or Q_0, for N at hexagonal or cubic sites, respectively; see Fig. 1), and the latter process—to phonon replicas in the PL spectrum. The shift of the zero-phonon line (P_0 or Q_0) from the so-called excitonic band gap[12] is equal to the binding energy of the exciton to the impurity atom. According to the empirical Haynes rule,[13] the exciton binding energy is roughly proportional to the ionization energy of the impurity atom. Therefore, the difference in the binding energies of excitons bound to N atoms at the two inequivalent sites in the unit cell of 4*H*-SiC (8.6 and 21.6 meV for the hexagonal and cubic sites, respectively) is an indication of a significant difference in their ionization energies. The values above follow from the PL spectrum as the difference between the excitonic band gap, E_x, and the corresponding zero-phonon line (P_0 or Q_0). Indeed, the ionization energy for the N donor at hexagonal (cubic) site in 4*H*-SiC is estimated to be around 45–52 (92–100) meV, respectively.[14]

Furthermore, a consequence of the different exciton binding energies is that mainly the phonon replicas of the ''more shallow'' P_0 line are observed in the spectrum. (Some of them are denoted in Fig. 1 as P_{xx}, where the subscript *xx* is the approximate energy of the phonon involved in the recombination.) The physical reason for this is quite simple: the excitons are bound to the ''shallower'' N atom at the hexagonal site rather weakly, so the interaction is weak and the probability for phonon-assisted recombination is higher than that for recombination involving an interaction with the impurity atom itself. That is why P_0 is rather weak, but its replicas are not. On the other hand, the excitons are bound stronger to N at the cubic site, which leads to a higher probability for recombination with transferring the excess momentum to the impurity atom. This is reflected in the much higher intensity of Q_0 with respect to P_0, and in the almost absent replicas of the Q_0 line. Actually, as will be seen, some of the strongest replicas of the Q_0 line are observed in the spectrum, but their intensities are negligible if compared to that of the same replicas from the P_0 line.

The free-exciton recombination can be regarded as an ultimate case of the same mechanism, when there is no binding at all. Consequently, only phonon-assisted recombination is allowed. In practice, however, due to the presence of defects and impurities in the real crystals, the zero-phonon free-exciton line (ZPFE) has been observed in indirect band-gap semiconductors (see, for instance, Ref. 15, for the case of Si). We also observe it, although very weakly, in both 4*H*- and 6*H*-SiC. Its appearance could be explained as due to the fact that some defects could serve in the accommodation of the excess momentum.[16] Thus, the observation of the ZPFE line provides a direct means for determining the excitonic band gap, which is otherwise obtained by comparison of the energy positions of the FE replicas with the N-BE replicas. For example, the energy distance between P_0 and its most intense phonon replica, noted in Fig. 1 as $P_{76.3}$, can be mea-

sured directly from the spectrum. It is 76.3 meV, the energy of the momentum conserving phonon. If we believe that the most intense FE replica is identified, which is quite unambiguous (see $I_{76.3}$ in Fig. 1), the excitonic band-gap position should lie 76.3 meV toward higher energies. The same holds for the other replicas of P_0 and the free exciton, and the energy position of the excitonic bandgap in 4*H*-SiC is determined to be $E_x \approx 3265$ meV (Ref. 17). It should be noted that the identification of the replicas of the FE is helped by their asymmetric lineshape arising from the Maxwellian velocity distribution,[18] in contrast to the symmetric line shape of the BE-related lines.

Thus, when a phonon is involved in the recombination of either a free, or a bound exciton, it is one of the 24 phonons at the *M* point. (4*H*-SiC has eight atoms per unit cell, which yields 24 ($=3\times8$) phonon branches.) This phonon is *created* during the recombination, and, besides the momentum, takes also a part of the energy of the exciton, equal to its own phonon energy. This has been exploited to determine the phonon energies for various polytypes in that point of the BZ where the minimum of the conduction band occurs. In combination with Raman spectroscopy, which yields information about phonon energies at the center Γ of the BZ, quite a lot of information on the phonon dispersion can be collected.[19] In the present paper we provide a more complete analysis of our experimental data for the phonon energies at the *M* point of the BZ in 4*H*-SiC, which is based on comparison of both sets of N-BE and FE replicas. Section II explains some experimental details concerning how to observe emission lines with polarizations both parallel and perpendicular to the crystal *c* axis in 4*H*-SiC. Section III gives a theoretical analysis and contains three parts. In Sec. III A, an analysis of the phonon symmetries at the *M* point is carried out. The results are then used in the Sec. III B to deduce the polarization selection rules for light emitted during recombination of N-BE or FE. Section III C presents a simplified model of the lattice dynamics of 4*H*-SiC which is used to gain information about the energy distribution of the phonons with different symmetries. Section IV presents the experimental results and a comparison with the theory.

II. EXPERIMENTAL CONSIDERATION AND DETAILS

The common experimental configuration (the near backscattering) used to record the low-temperature PL-spectrum of a CVD-grown epilayer is shown in Fig. 3(a). Because of the high value of the refractive index for the photon energies under consideration, this geometry is very close to the backscattering configuration, when the exciting laser beam and the light emitted from the crystal and received by the detector are almost collinear, but propagate in opposite directions.[20] Considering photon emission at a point inside the crystal, only those photons can exit the surface which are propagating at angles of incidence to the crystal surface smaller than the critical angle of total internal reflection, α_{cr}, satisfying the equation $\sin\alpha_{cr}=1/n$, where n is the refractive index of the layer. In 4*H*-SiC, $n\approx2.7$, which yields $\alpha_{cr}\approx22°$ (Ref. 21). If the *c* axis of the crystal is perpendicular to the surface of the layer, which is usually the case with (0001)-oriented samples, then only those photons can exit the layer surface which propagate at angles less than 22°

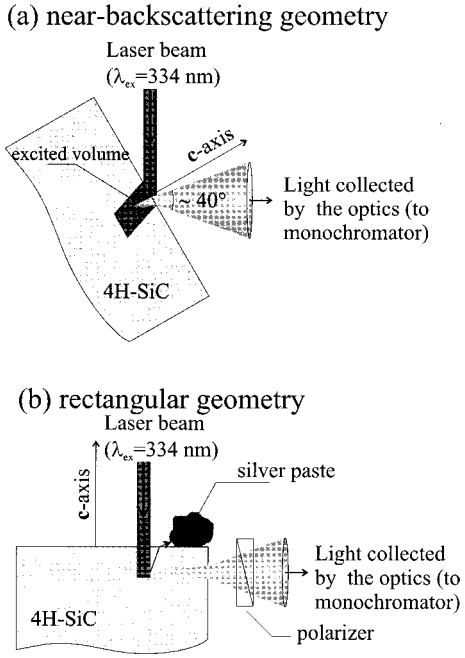

FIG. 3. The two experimental configurations used for recording the photoluminescence spectra. The values of the angles shown correspond to real experimental conditions.

with respect to the *c* axis. In practice only photons propagating within the angular aperture of the collecting optics are detected, which is typically around 40°, which corresponds to about 7° inside the crystal. Thus only photons propagating almost parallel to the *c* axis are detected. Due to the transverse nature of the electromagnetic waves they are polarized perpendicular to the *c* axis (we denote the polarization $\mathbf{E}\perp\mathbf{c}$ for this case, and $\mathbf{E}\parallel\mathbf{c}$ for the case of photons with polarization parallel to the *c* axis). For the same reason, the propagation of photons with $\mathbf{E}\parallel\mathbf{c}$ is confined in a plane perpendicular to the *c* axis.

Consequently, only spectral lines with $\mathbf{E}\perp\mathbf{c}$ can be observed in the common ''near-backscattering'' experiment from an (0001)-oriented face (*c* face). In order to observe lines polarized $\mathbf{E}\parallel\mathbf{c}$ as well either a different scheme like the one shown in Fig. 3(b) must be applied, or the ''backscattering'' luminescence should be recorded from an *a*-cut material [we will call ''*a* cut'' an orientation when the *c* axis lies in the surface of the layer, that is, either the prism face $(10\bar{1}0)$, or the *a*-face $(11\bar{2}0)$ orientation]. We used both methods to record the spectra containing lines with $\mathbf{E}\parallel\mathbf{c}$ polarization. Spectra of CVD epilayers grown on *a*-cut-material were reported earlier for 6*H*-SiC,[22] but the quality of the samples was much poorer than for a *c*-face material, and a careful analysis of the phonon replicas was not carried out.

The samples used in this study were all CVD grown epilayers. In the case of (0001)-oriented material, samples with different donor doping concentration were used, in order to observe or avoid the FE-related lines; in the case of very pure but compensated material, the FE lines are dominating the spectrum, which enabled us to record the FE-related replicas with both $\mathbf{E}\perp\mathbf{c}$ and $\mathbf{E}\parallel\mathbf{c}$ polarizations. Then the set of FE lines was compared with the N-BE lines, and this was used to judge which lines are due to phonon replicas.

The *a*-cut samples used were both $(10\bar{1}0)$ and $(11\bar{2}0)$ oriented, with almost the same quality as a *c*-face material. Although some contribution from the FE-related lines could be observed in the spectra, they were rather highly doped, and, consequently, mainly the N-BE related lines were investigated in this case.

All the spectra were recorded at 2 K with a double SPEX 1404 ($f=0.75$ m) monochromator, with a resolution of 0.4 Å, or better. The 334-nm UV line of an Ar^+-ion laser was used for excitation, with a power of 10 mW. In the case of the 90° experimental geometry (we call it briefly rectangular geometry) shown in Fig. 3(b), the laser beam was not focused on the sample in order to avoid the thermal-induced broadening of the FE lines. The resulting power density at the surface of the sample was less than 0.1 W/cm^2 (in the case of focused beam and backscattering geometry, used for the *a*-cut samples, it is about 20 W/cm^2). When a rectangular geometry was used, the possible contribution of photons with $\mathbf{E}\perp\mathbf{c}$ exiting the surface was blocked with a small heap of silver paste as shown in Fig. 3(b), and the light emitted through the edge of the sample was analyzed with a polarizer transmitting the desired polarization ($\mathbf{E}\perp\mathbf{c}$, or $\mathbf{E}\|\mathbf{c}$).

III. THEORETICAL BACKGROUND

This section provides the group-theoretical analysis necessary to understand the experimental results. First, the symmetry analysis of the phonons at the *M* point of the BZ is carried out. Afterwards, we establish the polarization selection rules for the phonon replicas and the zero-phonon lines. By ''polarization selection rules'' we mean the rules which correlate the polarization of the emitted photons with the symmetry of the states involved in the recombination process. However, the group-theoretical analysis does not in any way relate the symmetry of the phonons and their energies. That is why a lattice-dynamical model with the covalent bonding described by potential of Tersoff's type[23] is presented at the end of this section, and used to obtain more information about the symmetry of the phonons below and above the energy gap in the phonon spectrum of 4*H*-SiC.

A. Symmetry of the phonons at the *M* point

It is well known that the phonons at a certain point in the BZ can be classified by symmetry, that is, every phonon can be labeled with one of the irreducible representations of the group of the **k** vector at this point. Our goal now is to carry out this classification for the specific case of the phonons at the *M* point.

The group of the wave vector $\mathbf{k}_M$, corresponding to the *M* point of the BZ, is C_{2v}. It contains four of the 12 nontranslational symmetry operations of the space group C_{6v}^4, namely, *E* (the identity transformation), C_2, σ_v, and σ_v' [see Fig. 2(b)]; C_2 is equivalent to the Γk_z axis, $\sigma_v\perp\Gamma k_x$, and σ_v' is equivalent to the $A\Gamma ML$ plane. The four irreducible representations of C_{2v} are all one dimensional, and are listed in Table I. Thus there is no symmetry-based degeneracy of the phonon energies at the *M* point, and the matrix representations are identical to the characters.

The group-theoretical technique for determination of the numbers of phonons of given symmetry (M_1, M_2, M_3, or M_4) was described in detail in Ref. 24. For the sake of completeness, here we give a brief summary of the application of that technique to our particular case of the *M* point in the BZ of 4*H*-SiC.

TABLE I. The irreducible representations of C_{2v}, the group of the wave vector at the *M* point.

C_{2v} (*M* point)	E	C_2	σ_v	σ_v'
M_1	1	1	1	1
M_2	1	−1	1	−1
M_3	1	1	−1	−1
M_4	1	−1	−1	1

A 24-dimensional representation $\Gamma^{\rm disp}$ (called the displacement representation) can be constructed in the following way. Let us introduce a 24-dimensional vector **c**, the first three components of which are the *x*, *y*, and *z* projections of the displacement of atom No. 1, the next three components are the corresponding projections of the displacement of atom No. 2, etc. This is exactly the same way in which the eigenvectors of the dynamical matrix represent the displacements of the atoms corresponding to the normal modes (see, for example, Ref. 25). Let us think of each symmetry operation as acting on the displacements of the atoms, instead of on the atoms themselves. Then the result of the symmetry operation *T* on the vector **c** will be another vector **c**′, which can be written $\mathbf{c}'=\Gamma^{\rm disp}(T)\cdot\mathbf{c}$. Obviously, the set of matrices $\{\Gamma^{\rm disp}(T),\ T\in C_{2v}\}$ forms a (reducible) representation of the group of the wave vector (C_{2v} in our case), and it is quite straightforward to see that this representation can be presented as a direct matrix product

$$\Gamma^{\rm disp}(T)=p(T)\otimes R(T), \tag{1}$$

where $p(T)$ is the so-called permutation matrix for the operation *T* (the permutation matrix is a matrix containing 0's and 1's, and storing information about where each atom is going when the crystal is subjected to the operation *T*), and $R(T)$ is the ordinary 3×3 orthogonal matrix representing the rotation corresponding to the operation *T*. [Both sets, $\{p(T)\}$ (eight dimensional) and $\{R(T)\}$ (three dimensional) form also representations, called permutation and vector representations, respectively.] The character $\chi^{\rm disp}(T)$ of $\Gamma^{\rm disp}(T)$ is the product of the characters $u(T)$ and $r(T)=\pm(1+2\cos\vartheta)$ of $p(T)$ and $R(T)$, respectively. Here ϑ is the angle of rotation corresponding to $R(T)$, and the sign + (−) refers to proper (improper) rotation.

The displacement representation is completely reducible, that is, there exists a 24-dimensional unitary matrix *U* which transforms all $\Gamma^{\rm disp}(T)$ into a direct matrix sum of the irreducible representations M_p, $p=1$, 2, 3, and 4, listed in Table I,

$$U^{-1}\Gamma^{\rm disp}(T)U=\Gamma'(T)\equiv\sum_{p=1}^{4}\oplus n_pM_p(T). \tag{2}$$

The multiplicity of appearance of each of the representations M_p in the decomposition (2) of $\Gamma^{\rm disp}$, namely, n_p, is the number of phonons which transform as M_p. Here by ''a phonon transforming as M_p'' we mean that the eigenvectors

of the dynamical matrix constituted by the atomic displacements corresponding to a normal mode associated with this phonon transform as $M_p(T)$ under the symmetry operation T. In our case, when the representations are all one dimensional, this means that the symmetry operation T transforms the eigenvector $\mathbf{c}$ into the vector $M_p(T)\cdot\mathbf{c}=\pm\mathbf{c}$.

The numbers n_p, i.e., the numbers of phonons transforming as M_p, can be found using the well-known formula[24]

$$n_p=\tfrac{1}{4}\sum_{T\in C_{2v}}\chi^{\mathrm{disp}}(T)\chi^{p}(T)^*, \tag{3}$$

where $\chi^{\mathrm{disp}}(T)$ is the character of $\Gamma^{\mathrm{disp}}(T)$, and $\chi^{p}(T)^*$ is the complex conjugate of the character of the irreducible representation $M_p(T)$, in this particular case, $M_p(T)$ itself. The coefficient $\frac{1}{4}$ is the inverse of the order of the group C_{2v}. One then obtains that $n_1=8$, $n_2=4$, $n_3=4$, and $n_4=8$. Thus Eq. (2) implies that

$$\Gamma^{\mathrm{disp}}(T)\leftrightarrow\Gamma'(T)=8M_1(T)\oplus4M_2(T)\oplus4M_3(T)\oplus8M_4(T).$$

The sign $\leftrightarrow$ means ''is equivalent to.'' In the following we will omit for brevity the dependence on the group element T, so that, when written in terms of representations, the formula above can be expressed as

$$\Gamma^{\mathrm{disp}}\approx\Gamma'=8M_1\oplus4M_2\oplus4M_3\oplus8M_4. \tag{4}$$

This result will be used in Sec. III B in the analysis of the polarization selection rules.

It is worthwhile to recall here that, as can be seen from Eq. (2), the columns of the matrix U have the same symmetry as the eigenvectors of the dynamical matrix (or briefly the eigenvectors) in the sense that the first $n_1=8$ columns of U transform as M_1, the next $n_2=4$ columns as M_2, etc. If we denote by $\mathbf{u}^{p,r}$ and $\mathbf{c}^{p,r}$, $r=1,2,\ldots,n_p$, the columns of U and the eigenvectors, respectively, which transform as M_p, then they are related by a linear transformation

$$\mathbf{c}^{p,r}=\sum_{k=1}^{n_p}\alpha_{rk}\mathbf{u}^{p,k},\quad r=1,2,\ldots,n_p. \tag{5}$$

The vectors $\mathbf{u}^{p,r}$ ($p=1,\ldots,4$, $r=1,\ldots,n_p$) are called symmetry modes. Unlike the eigenvectors, the explicit form of which depends on the lattice dynamical model employed for their calculation,[26] the symmetry modes are determined only by the symmetry. For any given representation M_p, the sets of n_p vectors $\{\mathbf{c}^{p,r}\}$ and $\{\mathbf{u}^{p,r}\}$ can be regarded as orthogonal bases in one and the same subspace, namely, the subspace of all the vectors transforming as M_p. We will use this information plus the explicit form of the matrix U in order to draw some conclusions concerning the energy distribution of the phonons of given symmetry in Sec. III C,

We will finish this section by finding the matrix U bringing the displacement representation Γ^{disp} into the direct sum form [see Eq. (2)]. This can be done by means of the projection operators technique.[24] Using this technique, the columns of U, i.e., the vectors $\mathbf{u}^{p,r}$, can be presented as linear combinations of the Cartesian orthonormal basis unit vectors $\mathbf{v}_m$. In our case these are 24-dimensional vectors, the mth component of $\mathbf{v}_m$ ($m=1,2,\ldots,24$) being 1, and all the other components are zero (see also Ref. 24 for details). One can then obtain the following results, for our particular case of the M-point. Transforming as M_1 (the first eight columns of U),

$$\mathbf{u}^{1,1}=(\mathbf{v}_1-\mathbf{v}_4)/\sqrt{2},\quad \mathbf{u}^{1,2}=(\mathbf{v}_3+\mathbf{v}_6)/\sqrt{2},$$

$$\mathbf{u}^{1,3}=(\mathbf{v}_7-\mathbf{v}_{10})/\sqrt{2},\quad \mathbf{u}^{1,4}=(\mathbf{v}_9+\mathbf{v}_{12})/\sqrt{2},$$

$$\mathbf{u}^{1,5}=(\mathbf{v}_{13}-\mathbf{v}_{16})/\sqrt{2},\quad \mathbf{u}^{1,6}=(\mathbf{v}_{15}+\mathbf{v}_{18})/\sqrt{2},$$

$$\mathbf{u}^{1,7}=(\mathbf{v}_{19}-\mathbf{v}_{22})/\sqrt{2},\quad \mathbf{u}^{1,8}=(\mathbf{v}_{21}+\mathbf{v}_{24})/\sqrt{2}.$$

Transforming as M_2 (the next four columns of U),

$$\mathbf{u}^{2,1}=(\mathbf{v}_2+\mathbf{v}_5)/\sqrt{2},\quad \mathbf{u}^{2,2}=(\mathbf{v}_8+\mathbf{v}_{11})/\sqrt{2},$$

$$\mathbf{u}^{2,3}=(\mathbf{v}_{14}+\mathbf{v}_{17})/\sqrt{2},\quad \mathbf{u}^{2,4}=(\mathbf{v}_{20}+\mathbf{v}_{23})/\sqrt{2}.$$

Transforming as M_3 (the next four columns of U),

$$\mathbf{u}^{3,1}=(\mathbf{v}_2-\mathbf{v}_5)/\sqrt{2},\quad \mathbf{u}^{3,2}=(\mathbf{v}_8-\mathbf{v}_{11})/\sqrt{2},$$

$$\mathbf{u}^{3,3}=(\mathbf{v}_{14}-\mathbf{v}_{17})/\sqrt{2},\quad \mathbf{u}^{3,4}=(\mathbf{v}_{20}-\mathbf{v}_{23})/\sqrt{2}. \tag{6}$$

Transforming as M_4 (the last eight columns of U),

$$\mathbf{u}^{4,1}=(\mathbf{v}_1+\mathbf{v}_4)/\sqrt{2},\quad \mathbf{u}^{4,2}=(\mathbf{v}_3-\mathbf{v}_6)/\sqrt{2},$$

$$\mathbf{u}^{4,3}=(\mathbf{v}_7+\mathbf{v}_{10})/\sqrt{2},\quad \mathbf{u}^{4,4}=(\mathbf{v}_9-\mathbf{v}_{12})/\sqrt{2},$$

$$\mathbf{u}^{4,5}=(\mathbf{v}_{13}+\mathbf{v}_{16})/\sqrt{2},\quad \mathbf{u}^{4,6}=(\mathbf{v}_{15}-\mathbf{v}_{18})/\sqrt{2},$$

$$\mathbf{u}^{4,7}=(\mathbf{v}_{19}+\mathbf{v}_{22})/\sqrt{2},\quad \mathbf{u}^{4,8}=(\mathbf{v}_{21}-\mathbf{v}_{24})/\sqrt{2}.$$

The symmetry modes from Eq. (6) are presented as displacements of the atoms in the unit cell in Fig. 4.

B. Selection rules for free and nitrogen-bound exciton recombination in 4*H*-SiC

Before embarking on the exciton recombination selection rules it is necessary to know the positions and symmetries of the relevant band extrema for 4H-SiC. This information, which will be recapitulated here for convenience, has been presented in greater detail in Refs. 27 and 11. The labeling (i.e., the subscripts) of the irreducible representations within the present paper is the same as that used by Koster *et al.*[28]

According to the symmetry classification of the energy bands,[11] the conduction-band minimum has M_4 symmetry (see Table I), and is nondegenerate when excluding spin. The top of the valence bands has its maximum at the Γ point. If spin-orbit interaction is neglected, the valence-band maximum is twofold degenerate (fourfold if the spin degeneracy is included), and transforms as the two-dimensional Γ_5 representation of the point symmetry group C_{6v}. When spin-orbit interaction is taken into account, this fourfold degeneracy splits up into two twofold (spin) degenerate states of Γ_9 and Γ_7 symmetry in the double group C_{6v} of C_{6v}. The uppermost valence band state has Γ_9 symmetry and is higher than the Γ_7 state by the spin-orbit splitting, which is around 8 meV. When a substitutional N atom is present in the lattice, the point-group symmetry is reduced from C_{6v} to C_{3v}.

The selection rules will be based on the golden rule expression for the transition probability w_{fi} per unit time for

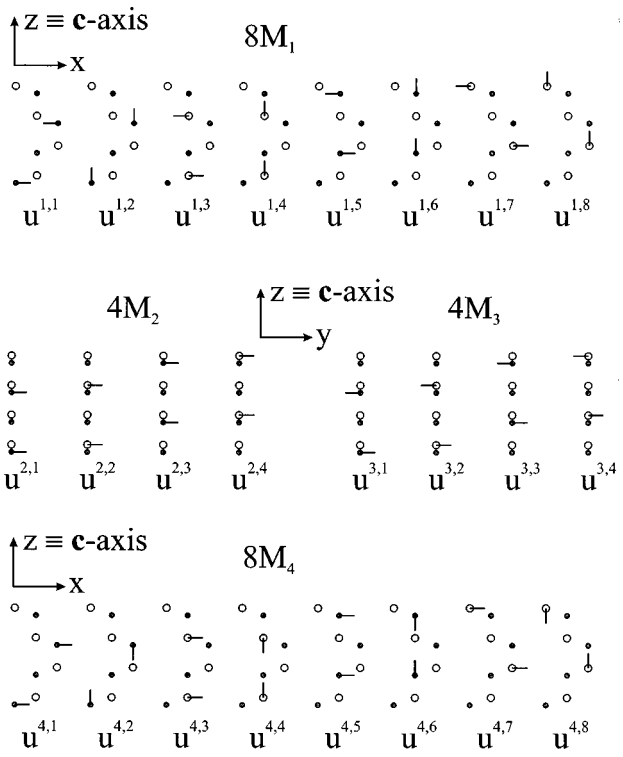

FIG. 4. The symmetry modes at the *M* point of the Brillouin zone of 4*H*-SiC represented as displacements of the atoms in the unit cell, and labeled according to Eq. (6). The atoms are represented by dots, smaller for C, and larger for Si. The modes are sorted by symmetry, so that all M_1 and M_4 modes have displacements lying in the *xOz* plane [cf. Fig. 2(a)], and the atoms are viewed in this plane, whereas all M_2 and M_3 modes have only displacements along the *Oy* axis, and are therefore viewed in the *yOz* plane.

transitions from an initial state $|i\rangle$ with total energy E_i to a final state $|f\rangle$ with total energy E_f,

$$w_{\mathrm{fi}}=\frac{2\pi}{\hbar}\,|H_{\mathrm{fi}}^{(n)}|^2\,\delta(E_f-E_i), \tag{7}$$

where, to first order $(n=1)$,

$$H_{\mathrm{fi}}^{(1)}=\langle f|\Delta H|i\rangle, \tag{8}$$

or, to second order $(n=2)$,[29,30]

$$H_{\mathrm{fi}}^{(2)}=\sum_{\nu}\frac{\langle f|\Delta H|\nu\rangle\langle\nu|\Delta H|i\rangle}{E_i-E_\nu}. \tag{9}$$

Here $|v\rangle$ are virtual states, and ΔH is the perturbation causing the transition.

1. Radiative zero-phonon recombination of N-bound excitons

The N-bound exciton is regarded as a four-particle complex with the two electrons (one from the N donor and the other from the exciton) in the same spatial, effective-mass-like state, obeying the Pauli exclusion principle, and a hole, also regarded as effective-mass-like.

Let us consider first a free electron existing in the environment of C_{6v} symmetry. The three wave functions for the electron states of M_4 symmetry, corresponding to the three equivalent minima in the BZ, can be combined linearly to form degenerate states of Γ_4 (one dimensional) and Γ_5 (two dimensional) symmetry in the point symmetry group C_{6v}. In the presence of a N atom, the symmetry is lowered to C_{3v}. In this point group the valley-orbit interaction will split this degeneracy. According to the compatibility relations in Ref. 28, $C_{6v}:\Gamma_4\rightarrow C_{3v}:\Gamma_2$ and $C_{6v}:\Gamma_5\rightarrow C_{3v}:\Gamma_3$. Thus the effective-mass-like substitutional donor wave functions in 4*H*-SiC will have Γ_2 or Γ_3 symmetry in the group C_{3v}, in analogy with the A_1, *E*, and T_2 symmetries for donors in Si (point symmetry group T_d). At this point, however, we do not know whether the Γ_2 state or the Γ_3 state is lower in energy and our analysis will therefore cover both possibilities. In the rest of this paragraph the symmetry labels will be with respect to the group C_{3v} or its double group $\bar{C}_{3v}$ unless otherwise stated.

To include the spin we form the direct product of Γ_2 and Γ_3 with the spin representation[28] $D_{1/2}$. This gives $\Gamma_2\times D_{1/2}=\Gamma_4$ (two-dimensional) and $\Gamma_3\times D_{1/2}=\Gamma_4\oplus\Gamma_{56}$, where Γ_{56} (two-dimensional) actually consists of two time-reversal (Kramers) degenerate one-dimensional representations, $\Gamma_{56}=\Gamma_5\oplus\Gamma_6$. Thus, the two electrons in the complex can each be either in a state of Γ_4 symmetry or in a state of Γ_{56} symmetry in the double group $\bar{C}_{3v}$.

The next step will be to form the two-electron states that satisfy the Pauli exclusion principle, i.e., which are antisymmetric with respect to interchange of electron coordinates:

$$\Gamma_4\times\Gamma_4=\Gamma_1\oplus\Gamma_2\oplus\Gamma_3, \tag{10a}$$

$$\Gamma_{56}\times\Gamma_{56}=(\Gamma_5\oplus\Gamma_6)\times(\Gamma_5\oplus\Gamma_6)=2\Gamma_1\oplus2\Gamma_2. \tag{10b}$$

Using the coupling coefficients tabulated in Ref. 28, we find that only the state of Γ_1 symmetry in Eq. (10a) and one of the states of Γ_1 symmetry in Eq. (10b) satisfy the Pauli exclusion principle. Thus, no matter whether Γ_4 or Γ_{56} is lower in energy, the two-electron state has Γ_1 symmetry.

As noted earlier, the top of the valence band has Γ_9 symmetry in the double group $\bar{C}_{6v}$. In the double group $\bar{C}_{3v}$ this is compatible with Γ_{56} symmetry. We thus conclude that the bound exciton has $\Gamma_{56}(=\Gamma_1\times\Gamma_{56})$ symmetry in the double group $\bar{C}_{3v}$. Since the exciton state is the initial state before recombination [the state $|i\rangle$ in Eq. (8)] we can thus write $|i\rangle\leftrightarrow\Gamma_{56}$, where the symbol $\leftrightarrow$ means ''transform as.''

The final state $|f\rangle$ in Eq. (8) after recombination is just the isolated donor state. As has already been seen, there are two possible candidates, $|f\rangle\leftrightarrow\Gamma_4$ or $|f\rangle\leftrightarrow\Gamma_{56}$. Furthermore, the dipole operator ΔH_ω can transform either as the Γ_1 representation (for the photon polarization vector $\mathbf{E}\|\mathbf{c}$ where $\mathbf{c}$ is the hexagonal *c* axis) or as the Γ_3 representation (for $\mathbf{E}\perp\mathbf{c}$, i.e., in the conventional *xy* plane). We now obtain the following selection rules:

$$\mathbf{E}\|\mathbf{c}:\quad \Delta H_\omega|i\rangle\leftrightarrow\Gamma_1\times\Gamma_{56}=\Gamma_{56}, \tag{11a}$$

$$\mathbf{E}\perp\mathbf{c}:\quad \Delta H_\omega|i\rangle\leftrightarrow\Gamma_3\times\Gamma_{56}=2\Gamma_4. \tag{11b}$$

Hence, in 4*H*-SiC the photons emitted in the direct radiative recombination of the N-BE will either be polarized parallel or perpendicular to *c*. According to our experiments (see

below), the zero-phonon lines (P_0 and Q_0) are polarized $\mathbf{E}\perp\mathbf{c}$, which allows us to conclude that the N-donor ground state has Γ_4 symmetry.

2. Radiative phonon-assisted recombination of free electrons and holes

For the sake of presentation we first consider the recombination of a *free* electron at the bottom of the conduction band with a *free* hole at the top of the valence band in a perfect 4*H*-SiC crystal. In order to conserve both energy and crystal momentum it is necessary to consider the second order process in Eq. (9) with

$$\Delta H=\Delta H_\omega+\Delta H_\Omega, \tag{12}$$

where ΔH_ω describes the electron-photon interaction, and ΔH_Ω describes the electron-phonon interaction. Neglecting two-photon as well as two-phonon processes, we obtain, from Eq. (9)

$$H_{\rm fi}^{(2)}=\sum_{\nu_1}\frac{\langle f|\Delta H_\omega|\nu_1\rangle\langle\nu_1|\Delta H_\Omega|i\rangle}{E_i-E_{\nu_1}}+\sum_{\nu_2}\frac{\langle f|\Delta H_\Omega|\nu_2\rangle\langle\nu_2|\Delta H_\omega|i\rangle}{E_i-E_{\nu_2}}. \tag{13}$$

For the energy denominators in Eq. (13) we have, quite generally,

$$E_i=\varepsilon_i+\sum_\alpha n_\alpha\hbar\omega_\alpha+\sum_\beta N_\beta\hbar\Omega_\beta, \tag{14}$$

where ε_i denotes the energy states of the initial electronic system, $n_\alpha(N_\beta)$ is the number of photons (phonons) of energy $\hbar\omega_\alpha(\hbar\Omega_\beta)$ in the initial state before recombination. Since a phonon and a photon are created during the recombination we must consider only photon and phonon emission. Hence we have

$$E_f=\varepsilon_f+\sum_\alpha n_\alpha\hbar\omega_\alpha+\hbar\omega+\sum_\beta N_\beta\hbar\Omega_\beta+\hbar\Omega, \tag{15}$$

where ε_f is the energy of the final electronic system, and $\hbar\omega$ ($\hbar\Omega$) is the energy of the emitted photon (phonon). In the first summation in Eq. (13) the virtual states $|\nu_1\rangle$ are connected to the initial state $|i\rangle$ through phonon emission. Then

$$E_{\nu_1}=\varepsilon_{\nu_1}+\sum_\alpha n_\alpha\hbar\omega_\alpha+\sum_\beta N_\beta\hbar\Omega_\beta+\hbar\Omega. \tag{16}$$

In the second summation in Eq. (13) the virtual states $|\nu_2\rangle$ are connected to the initial state through photon emission. Hence

$$E_{\nu_2}=\varepsilon_{\nu_2}+\sum_\alpha n_\alpha\hbar\omega_\alpha+\hbar\omega+\sum_\beta N_\beta\hbar\Omega_\beta. \tag{17}$$

Using these results in Eqs. (7) and (13), we obtain

TABLE II. Group-theoretical information used to analyze the first summation in Eq. (18) with $|i\rangle\leftrightarrow M_4$ in the space group C_{6v}^4. The first column enumerates the possible symmetries of the phonon operator ΔH_Ω, and the second column the possible symmetries of the virtual states $|\nu_1\rangle$ for allowed transitions. The third column shows the possible symmetries of the photon dipole operator ΔH_ω for light polarized perpendicular and parallel to *c*. The fourth column shows the possible symmetries of the final state at Γ. The symbol × indicates a direct product, and ⊕ a direct sum.

ΔH_Ω	$\lvert\nu_i\rangle$	ΔH_ω	$\Delta H_\omega\times\lvert\nu_1\rangle$
M_1	$\Gamma_4\oplus\Gamma_5$	Γ_5	$\Gamma_6\oplus(\Gamma_1\oplus\Gamma_2\oplus\Gamma_6)$
		Γ_1	$\Gamma_4\oplus\Gamma_5$
M_2	$\Gamma_2\oplus\Gamma_6$	Γ_5	$\Gamma_5\oplus(\Gamma_3\oplus\Gamma_4\oplus\Gamma_5)$
		Γ_1	$\Gamma_2\oplus\Gamma_6$
M_3	$\Gamma_3\oplus\Gamma_5$	Γ_5	$\Gamma_6\oplus(\Gamma_1\oplus\Gamma_2\oplus\Gamma_6)$
		Γ_1	$\Gamma_3\oplus\Gamma_5$
M_4	$\Gamma_1\oplus\Gamma_6$	Γ_5	$\Gamma_5\oplus(\Gamma_3\oplus\Gamma_4\oplus\Gamma_5)$
		Γ_1	$\Gamma_1\oplus\Gamma_6$

$$w_{\rm fi}=\frac{2\pi}{\hbar}\left|\sum_{\nu_1}\frac{\langle f|\Delta H_\omega|\nu_1\rangle\langle\nu_1|\Delta H_\Omega|i\rangle}{\varepsilon_i-\varepsilon_{\nu_1}-\hbar\Omega}+\sum_{\nu_2}\frac{\langle f|\Delta H_\Omega|\nu_2\rangle\langle\nu_2|\Delta H_\omega|i\rangle}{\varepsilon_i-\varepsilon_{\nu_2}-\hbar\omega}\right|^2\times\delta(\varepsilon_f-\varepsilon_i+\hbar\omega+\hbar\Omega). \tag{18}$$

The first summation describes a transition of the electron from the initial state $|i\rangle$ at the bottom of the conduction band transforming as M_4 (i.e., $|i\rangle\leftrightarrow M_4$) to a virtual state at Γ through the emission of a phonon, followed by photon emission from the virtual state to the final state $|f\rangle$ at the top of the valence band having Γ_5 symmetry (i.e., $|f\rangle\leftrightarrow\Gamma_5$). The photon dipole operator ΔH_ω can either transform as Γ_5 for *xy*-polarized light (i.e., when the photon polarization vector $\mathbf{n}\perp\mathbf{c}$) or as Γ_1 for the *z*-polarized light (i.e., $E\|\mathbf{c}$). In the second summation, the electron in state $|i\rangle\leftrightarrow M_4$ makes a virtual dipole transition at the *M* point ($\Delta H_\omega\leftrightarrow M_2$ for *x*-polarized light, $\Delta H_\omega\leftrightarrow M_4$ for *y*-polarized light, and $\Delta H_\omega\leftrightarrow M_1$ for polarization $E\|\mathbf{c}$), and emits a phonon to reach the final state $|f\rangle\leftrightarrow\Gamma_5$.

Since the three inequivalent band minima are at the *M* point, and the valence-band maximum is at Γ, the phonons participating in the indirect transitions have M_1, M_2, M_3, or M_4 symmetry, i.e., the phonon operator ΔH_Ω transforms as M_1, M_2, M_3, or M_4. In Sec. III A we showed that there are eight phonons of M_1 symmetry, four phonons of M_2 symmetry, four phonons of M_3 symmetry, and eight phonons of M_4 symmetry.

Below we will analyze the transition probability in Eq. (18) from a group-theoretical point of view to find the selection rules. This requires considerations involving the entire space group.[10] In Table II we show the results of the group-theoretical analysis of the first summation in Eq. (18). The first column shows the possible symmetries of the phonons involved, and the second column shows the symmetries of the virtual states at Γ to which phonon-assisted transitions of the M_4 electron are allowed. The results in this column were

TABLE III. Group-theoretical information used to analyze the second summation in Eq. (18), with $|i\rangle \leftrightarrow M_4$ in the space group C_{6v}^4. The first column enumerates the possible symmetries of the phonon operator ΔH_Ω, and the second column the possible symmetries of the virtual states $|\nu_2\rangle$ for allowed transitions, obtained as the direct product indicated and with the polarization of the dipole operator ΔH_ω as indicated by x, y, and z. The fourth column shows the possible symmetries of the final state at Γ.

ΔH_Ω	$\|\nu_2\rangle \leftrightarrow \Delta H_\omega \times \|i\rangle$		$\Delta H_\Omega \times \|\nu_2\rangle$
	(x)	M_3	$\Gamma_2 \oplus \Gamma_6$
M_1	(y)	M_1	$\Gamma_1 \oplus \Gamma_6$
	(z)	M_4	$\Gamma_4 \oplus \Gamma_5$
	(x)	M_3	$\Gamma_4 \oplus \Gamma_5$
M_2	(y)	M_1	$\Gamma_3 \oplus \Gamma_5$
	(z)	M_4	$\Gamma_2 \oplus \Gamma_6$
	(x)	M_3	$\Gamma_1 \oplus \Gamma_6$
M_3	(y)	M_1	$\Gamma_2 \oplus \Gamma_6$
	(z)	M_4	$\Gamma_3 \oplus \Gamma_5$
	(x)	M_3	$\Gamma_3 \oplus \Gamma_5$
M_4	(y)	M_1	$\Gamma_4 \oplus \Gamma_5$
	(z)	M_4	$\Gamma_1 \oplus \Gamma_6$

obtained using the tables of Ref. 10 for the nonsymmorphic space group C_{6v}^4. (It should be noted that the labeling of the irreducible representations in Refs. 28 and 10 differs somewhat. For instance, in the group C_{6v} the Γ_5 and Γ_6 representations are interchanged, whereas in the group C_{2v} the representations M_2 and M_3 are interchanged.) The third column shows the symmetry of the dipole operator for the two polarization directions considered, and the fourth column the possible final states. Since $|f\rangle \leftrightarrow \Gamma_5$, only those transitions for which the Γ_5 representation can be found in the fourth column are allowed. Hence light with polarization $\mathbf{E} \perp \mathbf{c}$ can only be obtained with the participation of phonons of M_2 and M_4 symmetry, which should give rise to 12 spectral lines, whereas light with polarization $\mathbf{E} \| \mathbf{c}$ can only result from participation of phonons of M_1 and M_3 symmetry, thus also giving rise to 12 spectral lines.

In Table III we consider the corresponding results for the second kind of indirect transition (i.e., second summation) in Eq. (18). The first column again shows the symmetries of the phonons involved, and the second column shows the symmetries of the virtual states at M to which photon dipole transitions of the M_4 electron are allowed. The third column shows the possible final states, and was obtained using the tables in Ref. 10. As before, since $|f\rangle \leftrightarrow \Gamma_5$, only those transitions for which the Γ_5 representation can be found in the third column are allowed. It is then clear that the selection rules for the second kind of indirect transition in Eq. (18) are exactly the same as for the first kind. Thus we have found that the selection rules for free electron-hole recombination in $4H$-SiC stipulate that there are 12 phonon-assisted emission lines with polarization $\mathbf{E} \perp \mathbf{c}$, and 12 phonon-assisted emission lines with polarization $\mathbf{E} \| \mathbf{c}$.

In the group-theoretical analysis of the phonon-assisted recombinations above, we disregarded spin-orbit interaction, i.e., the analysis was based on the single groups rather than on the double (space) group. If the analysis is based on double groups it turns out that all formally possible transitions are in principle allowed. But since group theory does not distinguish between weak (which may be practically undetectable) and strong (easily detectable) transitions, and since the spin-orbit interaction, which splits the top of the valence bands and induces the use of double groups, can be imagined to have only a minor influence on the free electron and hole wave functions (recall that the spin-orbit interaction operator is zero outside the atomic cores), it is not surprising that the analysis based on single groups in this case can give a better description of reality.

3. Radiative phonon-assisted recombination of free and N-bound excitons in 4H-SiC

The analysis in Sec. III B 2 should also be applicable to phonon-assisted recombination of FE's: the FE wave functions can be regarded as being built up from effective-mass-like electron and hole wave functions with the symmetry of the conduction-band minimum and valence-band maximum, respectively. Furthermore, the FE exist in an environment having the full space-group symmetry of the perfect lattice.

For bound excitons, however, the situation is more complicated, since from a group-theoretical point of view the space group of the perfect crystal is no longer the appropriate basis for a group-theoretical analysis because of the presence of the impurity. One can argue, however, that if the exciton binding is relatively weak (less than 20–30 meV in our case), the exciton wave function is only slightly perturbed by the presence of the N donor, and consequently the selection rules for phonon-assisted recombination of the N-BE need not in practice differ appreciably from the selection rules for the FE. This seems to be supported by our experimental results since, as will be seen, the two sets of replicas, for the N-BE and the FE, are very similar to each other.

C. Model of lattice dynamics of 4H-SiC and distribution of phonons by energy

Here we present a simple lattice-dynamical model for calculating the phonon spectrum of $4H$-SiC. The full phonon-dispersion calculations along some high-symmetry directions of the BZ are briefly presented, although we do not aim here at a construction of a more precise model than those already presented by other authors (see, for instance, Ref. 26). Instead, our purpose is to obtain some general information relating the energies of the phonons and their symmetries, especially at the M point of the BZ. Our conclusions are based on some general physical observations illustrated by means of the lattice-dynamical model. However, we believe that a rigorous proof from a mathematical point of view is possible, although not performed here. The features pointed out in the following are common for any lattice dynamical model of $4H$-SiC.

Description of the model. For the short-range interactions between the atoms, we have used the expression for the energy in crystals with covalent bonds proposed by Tersoff.[23] In order to find the force constants necessary for constructing the dynamical matrix, a complete analytical evaluation of the second derivatives of the energy has been carried out. The parameters in the expression for the energy, which become the parameters determining the force constants responsible for the short-range interactions, are the same as those pro-

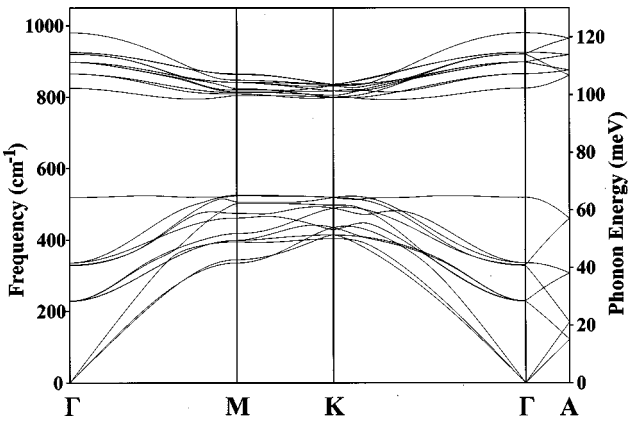

FIG. 5. The phonon dispersion in 4*H*-SiC along some high-symmetry directions of the Brillouin zone, as calculated in the frame of the lattice-dynamical model.

posed by Tersoff, and have not been optimized. The long-range Coulomb interactions between the ions have also been taken into account and evaluated by means of the Ewald method (see Ref. 25, and references therein), in order to reproduce the LO-TO splitting at the center of the BZ.

The phonon dispersion along some high-symmetry directions of the BZ produced by means of this model is shown in Fig. 5. The agreement between the model and the experimentally determined quantities, such as the phonon energies at the center (Γ) and the *M* point, and the value of the energy gap in the phonon dispersion, is not very good. However, we believe that a much more adequate description would be possible within this model if its parameters would be systematically adjusted, which has not been aimed at here since it has not been necessary for the current treatment.

The calculated atomic displacement fields at the *M* point and a graphics representation of the eigenvectors of the dynamical matrix are presented in Fig. 6. Each displacement configuration is labeled with the calculated phonon energy

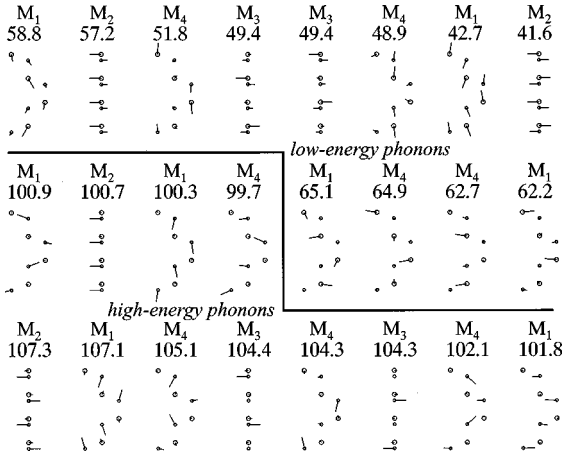

FIG. 6. The atomic displacement fields associated with the phonons at the *M* point, and representing the eigenvectors of the dynamical matrix. The atoms in the unit cell and their displacements are represented in the same way as in Fig. 4. Each displacement configuration is labeled with the corresponding calculated phonon energy and symmetry. The thick solid line separates the phonons above and below the energy gap in the phonon dispersion, called high- and low-energy phonons, respectively.

and the irreducible representation describing its symmetry. These ''symmetry labels'' can be obtained by calculating the scalar product between the eigenvectors and the symmetry modes. However, a much quicker way is provided by comparing the normal modes from Fig. 6 with the symmetry modes from Fig. 4. Each normal mode has displacements either in the *xOz* plane (therefore, it has M_1 or M_4 symmetry), or in the *yOz* plane (which means M_2 or M_3 symmetry). Furthermore, to distinguish, for example, M_2 from M_3 symmetry, it is sufficient to note whether the displacements of the equivalent atoms (say, 1 and 2) along the *Oy* axis have the same sign, or different signs (this distinguishes M_2 and M_3, respectively, as seen from Fig. 4). To distinguish M_1 from M_4, again the signs of the displacements of the equivalent atoms should be considered. If the signs of the components of these displacements along *Ox* coincide, then the symmetry is M_4 (and the components along the *Oz* axis necessarily have opposite signs), and vice versa. Of course, in all cases (not only at the *M* point), the vectors representing the displacements of the equivalent atoms have the same amplitude, but possibly different orientation.

Let us consider now the calculated displacement fields from Fig. 6. One can then make the following observations.

(1) There exists an energy gap in the phonon dispersion, and the numbers of phonon dispersion curves above and below it, are equal (12 above and 12 below, in our case). This seems to be a general property of all crystals constituted of two sublattices of different atoms (C and Si, in our case). The existence of energy gap for such compounds is discussed in Ref. 31, although, to our knowledge, a rigorous proof is still missing.

(2) Regarding the high-energy phonon branches (above the energy gap), one can notice that the displacements of the ''heavy'' (Si) atoms are much smaller than the displacements of the ''light'' (C) atoms. The physical reason is that the heavy (Si) atoms do not succeed in following the light (C) atoms, when the oscillation is with a ''high'' frequency (above the energy gap), and, therefore, their displacement is always smaller. We suggest now that all high-energy phonons include mainly the displacements of the lighter atoms in the binary compound (C in our case).

In what concerns the phonon branches below the band gap, one can see that the modes of vibration can be subdivided into two types, namely, normal modes in which the displacement of the heavy atoms is dominant, and modes when both the heavy and light atoms have significant displacement amplitudes. When only the heavy atoms move, the frequencies will be higher than in the case when pairs consisting of a heavy atom and the adjacent light atom move in phase; in the latter case the two atoms can be regarded as a single particle with a mass equal to the sum of the two masses, and, therefore, oscillating with still lower frequency. This is well illustrated in Fig. 6.

Thus, although the eigenvectors depend on the lattice-dynamical model employed, we have reasons to assume that the two properties we just pointed out are independent thereof, because any model should obey the general physical principles used to motivate our observations. Now, on the basis of these observations, we are able to derive some conclusions concerning the distribution of the phonons of each symmetry with energies above and below the energy gap by

symmetries, that is, conclusions concerning the numbers of phonons labeled with given irreducible representation above and below the energy gap. These conclusions are deduced here for the case of the M point in the BZ of $4H$-SiC, or any point on the line M-L, because these points have the same symmetry. However, the same idea can be employed in analyzing the phonon distribution by symmetry in many other cases, for different binary crystals. A further generalization of the ideas we use here, as well as rigorous proof of the conclusions we are going to make, are beyond the scope of this paper.

For definiteness, let us consider the phonons transforming as M_1. If we regard the corresponding eigenvectors $\mathbf{c}^{1,r}$ as linear combinations of the symmetry modes $\mathbf{u}^{1,r}$ ($r=1,\ldots,8$), then the second observation implies that the eigenvectors corresponding to phonons above the energy gap are mainly constituted of the vectors $\mathbf{u}^{1,1}$, $\mathbf{u}^{1,2}$, $\mathbf{u}^{1,5}$, and $\mathbf{u}^{1,6}$, i.e., the vectors which correspond to displacements of the C atoms. The contribution from $\mathbf{u}^{1,3}$, $\mathbf{u}^{1,4}$, $\mathbf{u}^{1,7}$, and $\mathbf{u}^{1,8}$ in these eigenvectors is negligible. If this latter contribution was exactly zero, then we obviously would be able to construct only four mutually orthogonal eigenvectors (let these be the vectors $\mathbf{c}^{1,1}$, $\mathbf{c}^{1,2}$, $\mathbf{c}^{1,3}$, and $\mathbf{c}^{1,4}$) which are linear combinations of the four vectors $\mathbf{u}^{1,1}$, $\mathbf{u}^{1,2}$, $\mathbf{u}^{1,5}$, and $\mathbf{u}^{1,6}$. Indeed, if any other vector is a linear combination of $\mathbf{u}^{1,1}$, $\mathbf{u}^{1,2}$, $\mathbf{u}^{1,5}$, and $\mathbf{u}^{1,6}$, then it can also be presented as a linear combination of $\mathbf{c}^{1,1}$, $\mathbf{c}^{1,2}$, $\mathbf{c}^{1,3}$, and $\mathbf{c}^{1,4}$, and, therefore, cannot be orthogonal to these vectors, i.e., cannot be an eigenvector. Moreover, it is easy to prove that if a vector is orthogonal to all of these four eigenvectors ($\mathbf{c}^{1,1}$, $\mathbf{c}^{1,2}$, $\mathbf{c}^{1,3}$, and $\mathbf{c}^{1,4}$), then it must be a linear combination of only $\mathbf{u}^{1,3}$, $\mathbf{u}^{1,4}$, $\mathbf{u}^{1,7}$, and $\mathbf{u}^{1,8}$, i.e., it belongs to the subspace spanned by the latter four vectors, comprising only displacements of the Si atoms. According to our second observation, such an eigenvector represents a phonon from a branch below the energy gap. Then we obviously obtain equal numbers of phonons having M_1 symmetry below and above the energy gap, and the same result applies to the rest of the phonons, transforming as M_2, M_3, and M_4. In this ideal case (which is *not* the reality), the phonons of given symmetry are equally distributed above and below the gap.

Let us extend our reasoning to the case of *real* eigenvectors. Let us regard the high-energy phonons (above the energy gap), when the contribution from the displacements of the ''heavy'' Si atoms in the phonons above the gap is not exactly zero, but small (Fig. 6). Let us again consider only one representation, say, M_1. According to observation 2, we can say that each of the eigenvectors describing the phonons above the gap ''almost'' belongs to the subspace spanned by the four vectors $\mathbf{u}^{1,1}$, $\mathbf{u}^{1,2}$, $\mathbf{u}^{1,5}$, and $\mathbf{u}^{1,6}$, and has negligible projections out of this space, namely, in the subspace spanned by the other four vectors $\mathbf{u}^{1,3}$, $\mathbf{u}^{1,4}$, $\mathbf{u}^{1,7}$, and $\mathbf{u}^{1,8}$. We have a reason to assume then that at most four of the eight eigenvectors transforming as M_1 can have this property, that is, have negligible contributions from $\mathbf{u}^{1,3}$, $\mathbf{u}^{1,4}$, $\mathbf{u}^{1,7}$, and $\mathbf{u}^{1,8}$, and being mutually orthogonal at the same time. This assumption leads to the conclusion that another eigenvector will necessarily have a significant contribution from at least one of the vectors $\mathbf{u}^{1,3}$, $\mathbf{u}^{1,4}$, $\mathbf{u}^{1,7}$, and $\mathbf{u}^{1,8}$, which means significant amplitude of vibration of the corresponding ''heavy'' Si atom, and, consequently, a phonon energy below the gap. This is illustrated in Fig. 6. All the eigenvectors corresponding to frequencies below the energy gap exhibit significant displacements for at least one pair of equivalent Si atoms.

If our assumption is valid, then it can be extended to each M_p, and it claims that at most half of the phonons transforming as M_p have energies above the gap. Actually, this implies that *exactly* half of the phonons have energies above and below the gap for each representation. For if we assume that the number of phonons for M_1, for instance, is less than four, then the number of phonons for some other representation M_p ($p\neq 1$) will be greater than $\frac{1}{2}n_p$ in order to complete the total number of phonons above the gap to 12. This contradicts with our conclusion that *at most* $\frac{1}{2}n_p$ of the phonons transforming as M_p belongs to the set of phonons above the energy gap.

Thus, we find that the phonons of each symmetry are equally distributed above and below the energy gap in the phonon dispersion. According to the deduced polarization rules, this in turn implies that one should expect equal numbers of phonon replicas for each polarization above and below the energy gap. In other words, we expect six phonon replicas with $\mathbf{E}\|\mathbf{c}$, and six with $\mathbf{E}\perp\mathbf{c}$, both above and below the energy gap. We now briefly summarize the theoretical results obtained.

(1) At the M point of the BZ, as well as along the M-L direction, the phonons are classified by symmetry, as follows: eight phonons transform as M_1, four as M_2, four as M_3, and eight as M_4. The phonons with M_1 and M_4 symmetries have displacements only in the xOz plane, and the phonons with M_2 and M_3 symmetries only along the Oy axis (see Figs. 4 and 6).

(2) According to the polarization selection rules derived in Sec. III B the zero-phonon lines for the N-bound excitons (P_0 and Q_0) are polarized $\mathbf{E}\perp\mathbf{c}$, if the ground state of the N donor has Γ_4 symmetry, which is also observed experimentally. However, if the ground state had the other possible symmetry, Γ_{56}, then the polarization of the zero-phonon lines would be $\mathbf{E}\|\mathbf{c}$, which is not observed experimentally. Thus, the experiment provides a direct evidence that the lowest (ground) state of the N donor has Γ_4 symmetry.

(3) Furthermore, the polarization selection rules for the phonon replicas of either the bound or free excitons imply that if the phonon accomplishing the momentum conservation is of M_1 or M_3 symmetry, the corresponding replica is polarized $\mathbf{E}\|\mathbf{c}$, whereas if the phonon has M_2 or M_4 symmetry, the replica is polarized $\mathbf{E}\perp\mathbf{c}$. Therefore, there are 12 phonon replicas with $\mathbf{E}\|\mathbf{c}$ polarization and 12 with $\mathbf{E}\perp\mathbf{c}$ polarization, for each set of phonon replicas (bound or free exciton).

(4) According to Sec. III C the number of phonons of given symmetry above and below the energy gap in the phonon dispersion is the same. Thus, one should expect to observe six phonon replicas with polarization perpendicular $\mathbf{c}$, and six with polarization parallel $\mathbf{c}$, both below and above the phonon energy gap.

We turn now to the experimental results and compare them to the theory.

IV. EXPERIMENTAL RESULTS AND COMPARISON TO THE THEORY

Three kinds of $4H$-SiC samples were investigated, which we refer to here as sample No. 1 with strong N-BE-related

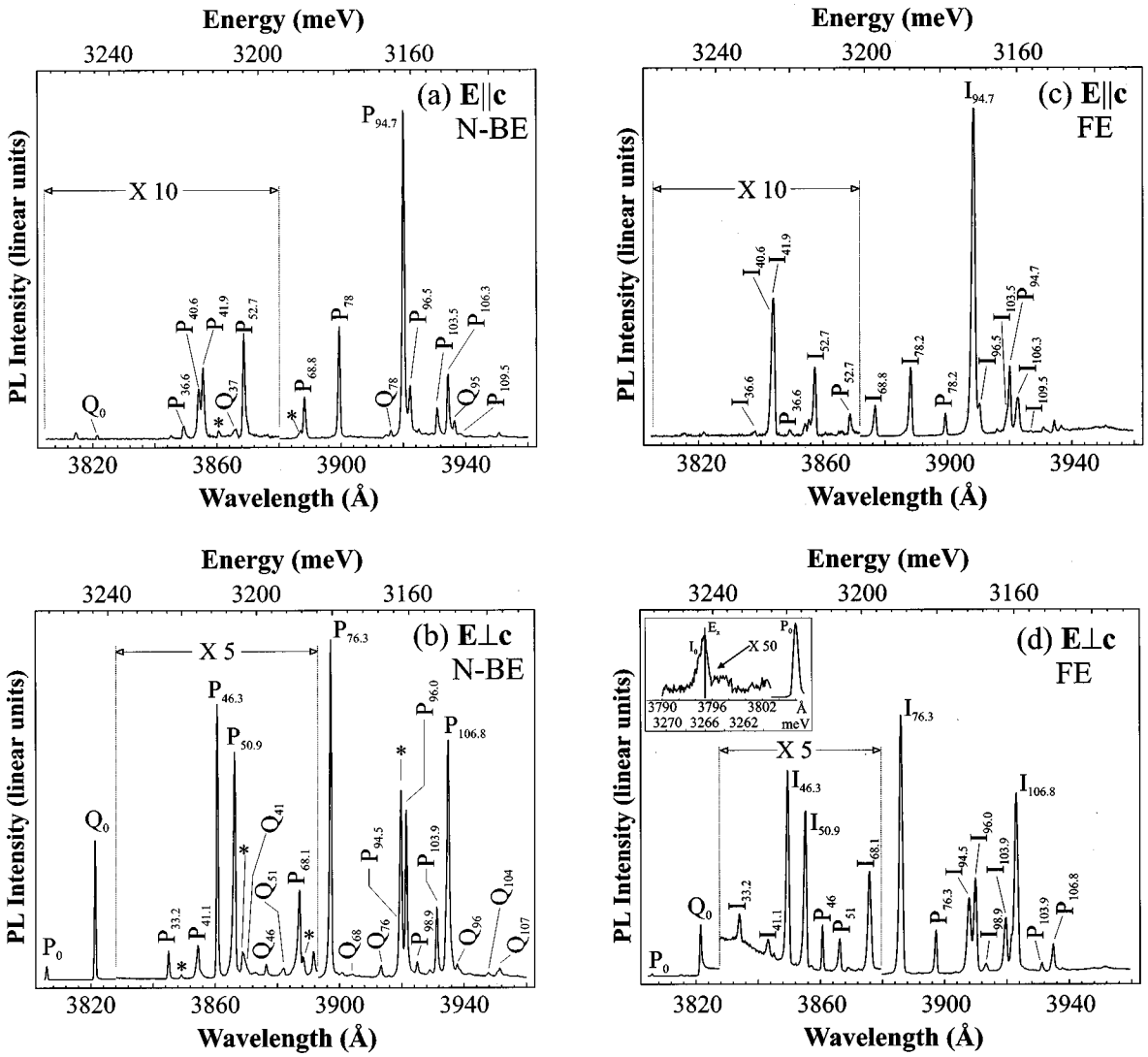

FIG. 7. Polarized PL spectra of sample Nos. 1(a) and 1(b) and 2(c) and 2(d), showing strong N-BE related lines, and FE related lines, respectively. (a) and (c) contain the lines, polarized parallel to *c*, (b) and (d) lines polarized perpendicular to *c*. The asterisks denote some residual lines from the other polarization. Note the change of the intensity scale in the low-energy part of the spectra.

luminescence and absent FE-related lines [*n*-type doping around $(2-5)\times10^{16}$ cm^{-3}], sample No. 2 with strong FE-related luminescence, and two *a*-cut samples, for both $(10\bar{1}0)$ and $(11\bar{2}0)$ orientations. For the first two cases, the rectangular geometry shown in Fig. 3(b) was used to record the polarized spectra through the edge of the sample, and for the *a*-cut samples the usual near-backscattering geometry was used [Fig. 3(a)].

The polarized spectra for sample Nos. 1 and 2 are shown in Fig. 7. We use the spectrum of sample No. 1 to obtain the phonon replicas of the BE (of the P_0 line), and that of sample No. 2 for the phonon replicas of the FE. Each of the replicas in the corresponding set is shifted with the energy of the phonon involved in the recombination from the corresponding zero-phonon line (P_0 for the set of the N-BE lines, and I_0, the ZPFE line, for the set of FE lines). As already discussed in Sec. I, I_0 is forbidden. However, it still can be observed in some samples, which provides direct evidence of the position of the excitonic band gap. One of our spectra for I_0 is shown in the inset of Fig. 7(d), where the excitonic band gap obtained in this work, $E_x=3266$ meV, is denoted with a vertical bar. It appears unshifted from E_x, at least within the accuracy of the experiment ($\approx$0.2–0.3 meV), which supports the conclusion that the energy taken from the momentum-conserving particle during the ''direct'' recombination of the FE is negligible. It is worth noting that we have observed the I_0 line also in 6*H*-SiC, and the typical asymmetric Maxwellian line shape of the FE-related lines is obvious for both polytypes, making the assignment of the observed line quite unambiguous. In 6*H*-SiC, I_0 also appears unshifted with respect to the calculated excitonic band gap ($\approx$3023 meV).

After thorough evaluation of the line positions in the polarized spectra and comparing the replicas of the bound and free excitons, we were able to derive 22 of the 24 replicas in 4*H*-SiC, 11 for the **E**$\perp$**c** polarization and 11 for the **E**$\parallel$**c** polarization. They are listed in Table IV together with the associated phonon energies. In Fig. 8, the same replicas are shown as narrow vertical lines with height proportional to the intensities of the real lines from the spectra, both for the free and bound excitons. One can see that the intensity distribution among the replicas is almost identical if we compare the free- and bound-exciton sets for each polarization.

TABLE IV. Phonon energies at the *M* point of 4*H*-SiC, polarization of the corresponding phonon replicas, and comparison with Ref. 32.

Phonon energies (meV)		
Ref. 32	Our data	Polarization
33.0	33.2	$E\perp c$
36.5	36.6	$E\|\|c$
40.6	40.6	$E\|\|c$
41.0	41.1	$E\perp c$
41.7	41.9	$E\|\|c$
46.1	46.3	$E\perp c$
50.8	50.9	$E\perp c$
52.7	52.7	$E\|\|c$
67.8	68.1	$E\perp c$
68.7	68.8	$E\|\|c$
76.6	76.3	$E\perp c$
78.5	78.0	$E\|\|c$
	Energy gap	
-	94.5	$E\perp c$
96.1	94.7	$E\|\|c$
97.3	96	$E\perp c$
97.8	96.5	$E\|\|c$
99.1	-	
100.3	98.9	$E\perp c$
101.6	-	
105.6	103.5	$E\|\|c$
106.3	103.9	$E\perp c$
108.2	106.3	$E\|\|c$
108.7	106.8	$E\perp c$
-	109.5	$E\|\|c$

For instance, if we consider $\mathbf{E}\perp\mathbf{c}$ polarization, the strongest replica in the spectrum of the free exciton is $I_{76.3}$, and $P_{76.3}$ is also most intense in the spectrum of the bound exciton. The next most intense replicas are I_{46} and P_{46}, and both lines have about 15% of the intensity of the $I_{76.3}$ and $P_{76.3}$ lines, respectively, and so on. *This rather accurate match of the relative intensities of the replicas in the BE and FE spectra supports the conclusion that the wave functions describing the bound exciton are quite similar to those of the free exciton*. In other words, the effective-mass approximation seems to be quite relevant in the description of both free and bound excitons to *N* excitons.

In Sec. III B we already discussed the polarization of the zero-phonon lines P_0 and Q_0. They are polarized perpendicular to *c* (see Fig. 7), which was the reason to conclude that the lowest N-donor state has Γ_4 symmetry. From the same figure it can be seen, however, that when recording the spectrum with $\mathbf{E}\|\mathbf{c}$ polarization, the lines polarized perpendicular to **c** do not vanish completely. We would like to point out that, apart from a possible disorientation of the polarizer, the ''opposite'' polarization may always be observed, due to a scattering of photons from some inhomogeneities in the crystal. This is also the most probable reason for seeing (after careful inspection) some weak contribution from the replicas with $\mathbf{E}\|\mathbf{c}$ polarization in the usual PL spectrum recorded in backscattering geometry (see Fig. 1).

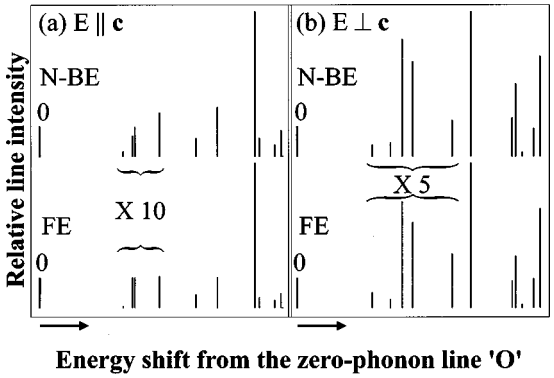

FIG. 8. Comparison between the relative intensities of the lines originating from the N-BE and FE recombination, obtained from Fig. 7. The set of replicas of P_0 is shown in the upper part of panels (a) and (b), for $E\|c$ and $E\perp c$, respectively, and the corresponding FE replicas are in the lower part.

We can now inspect the energy distribution of the phonons. A recent work[32] reported on phonon replicas in 4*H*-SiC, and we compare our results with this work in Table IV. Let us first consider replicas due to phonons with energies below the energy gap, which for 4*H*-SiC at the *M* point is approximately between 78 and 94 meV, as can be seen from the spectra, the table, and phonon dispersion calculations.[26] In this low-energy range, our results are in excellent agreement with Ref. 32. Some small discrepancies exist, however, and may be due to the way the spectra were recorded (in Ref. 32 the authors did not perform complete polarization measurements, and some close replicas with different polarization may overlap which causes an apparent shift of the lines). Another reason could be differences in material quality, since small shifts of the replicas and the zero-phonon lines are possible in a strained material. An early work[33] also supported the results from Table IV (the part below the gap). However, at that time, the results were misinterpreted as a proof that the minimum of the conduction band is not at the *M* point in 4*H*-SiC.

Furthermore, we observe 12 phonon replicas in the low-energy part (phonons below the gap), which means that we observe all of them. Moreover, six of them are polarized parallel to **c**, and six perpendicular to **c**. This is in agreement with our conclusion made in Sec. III C concerning the equal distribution of the phonons of each symmetry below and above the energy gap. Therefore we can deduce that the six replicas with $\mathbf{E}\|\mathbf{c}$ polarization are produced by four phonons of M_1 symmetry and two phonons of M_3 symmetry, whereas the other six replicas polarized $\mathbf{E}\|\mathbf{c}$ are due to two phonons of M_2 symmetry and four phonons of M_4 symmetry. At present, however, we do not have the means to decide exactly which replicas are due to phonons of a certain symmetry.

Let us consider now the phonon replicas due to phonons with energies above the energy gap ($>$94 meV), or, roughly speaking, the high-energy phonon replicas. First of all, the appearance of a systematic shift toward higher energies in the data from Ref. 32 with respect to our values becomes visible (it can already be noted in the low-energy part). It might be due to the difference in the conversion factors; to convert the wavelength to energy, we have used the formula

$E = 1.239\,493/\lambda(\mu\mathrm{m})$, which is obtained if the refractive index of standard air at wavelength 4000 Å is taken into account in the formula for vacuum: $E = 1.239\,856/\lambda_v(\mu\mathrm{m})$, where λ and λ_v are the measured wavelength values in air and vacuum, respectively. In Table IV, some further discrepancies can be seen which concern the assignment of some lines. There are several possible reasons for that, among which it is worth mentioning the following. The energy region containing these replicas also contains the spectrum arising from recombination of excitons by two-phonon processes. Thus the selection of the first-order phonon replicas is much more difficult in this region, and the comparison of the spectra of the BE and FE replicas becomes crucial in judging which lines are replicas, and which are not. All ten high-energy replicas reported by us here have been observed in both the BE and FE spectra. The specific ''asymmetric'' line shape of the FE-related replicas is also useful in the identification of the lines. Some strong replicas of the Q_0 line also fall within this region (we have identified and marked most of the Q_0 replicas in order to exclude them from consideration).

However, we only succeeded in finding ten of the 12 replicas in this region. By coincidence, in Ref. 32, ten replicas are also reported, although most of them are at different energies than ours. Five of these replicas observed by us are polarized parallel to *c*, and five perpendicular to *c*. Thus we ''miss'' two replicas in this region, one for each polarization direction. There are two possible reasons for this. First, there always exists a possibility for accidental degeneracy of the phonon energies, so the missing lines are not resolved from some of the others. Second, the ''missing'' replicas might be resolvable, but very weak. Thus, in 6*H*-SiC, for example, the less intense phonon replica of the FE at around 29 meV is about three orders of magnitude weaker than the most intense one (I_{77}).

Finally, the nonpolarized spectra of the *a*-cut samples recorded in the usual near-backscattering geometry are presented in Fig. 9. Note that the spectra for $(10\bar{1}0)$- and $(11\bar{2}0)$-oriented samples are very similar. This is not surprising if we take into account the existence of two equivalent directions in the (0001) plane. The slight difference in the spectra [slightly shifted and broadened lines in the $(10\bar{1}0)$ sample] is due to the difference in the sample quality. As expected, all $\mathbf{E}\|\mathbf{c}$ and $\mathbf{E}\perp\mathbf{c}$ replicas listed in Table IV can be seen in the usual spectra for these samples. The polarized spectra (not shown here) are not as accurate as the spectra in Fig. 7, that is, there is a significant residual contribution from the other polarization, because the geometry is not as well defined as in the case of rectangular geometry. Therefore, we regard these spectra as a confirmation of the attribution of the phonon replicas performed from the previous spectra.

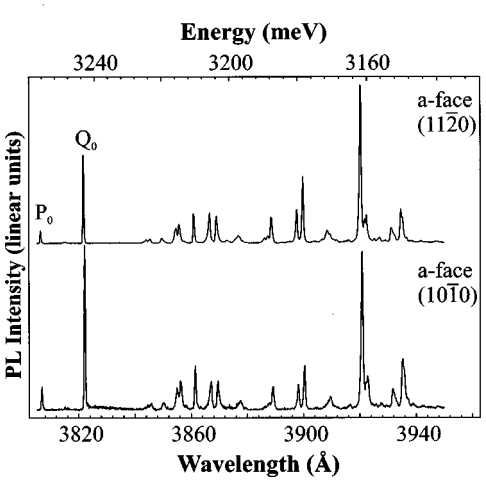

FIG. 9. PL spectra ($T = 2$ K) of *a*-cut CVD-grown samples, of $(11\bar{2}0)$ (upper curve), and $(10\bar{1}0)$ orientations. The spectra are nonpolarized, and obtained in the common near-backscattering geometry.

V. CONCLUSION

We have performed a complete analysis of the phonons at the *M* point of the Brillouin zone of 4*H*-SiC, starting with the classification of the phonons by symmetry, then deriving the polarization selection rules from a group-theoretical point of view, and applying these rules in the analysis of the experimental data. A lattice-dynamical model is used to illustrate our conclusions concerning the equal distribution of the phonons of given symmetry above and below the phonon energy gap. However, a further test of our observations, by means of other models of the lattice dynamics, would be very useful, since we believe that the features pointed out for our model in Sec. III C are actually independent of the model. The theoretical conclusions seem to be in excellent agreement with the experimental results.

ACKNOWLEDGMENTS

The authors gratefully acknowledge support from the Swedish Research Council for Engineering Sciences (TFR), the Swedish Foundation for Strategic Research (SSF), and ABB Corporate Research.

*Also at ABB Corporate Research, S-72 178 Västerås, Sweden.

†Present address: Cree Research, Inc., 2810 Meridian Parkway, Suite 176, Durham, NC 27713.

[1] O. Kordina, A. Henry, E. Janzén, C. H. Carter, Jr., in *Proceedings of the International Conference on Silicon Carbide, III-Nitrides and Related Materials, Stockholm*, edited by G. Pensl, H. Morkoç, B. Monemar, and E. Janzén (Trans Tech, Uetikon-Zuerich, Switzerland, 1998), p. 97; A. A. Burk, Jr., M. J. O'Loughlin, and S. S. Mani, in *ibid.*, p. 83.

[2] L. L. Clemen, R. P. Devaty, W. J. Choyke, A. A. Burk, Jr., D. J. Larkin, and J. A. Powell, Inst. Phys. Conf. Ser. **137**, 227 (1994).

[3] L. Patrick and W. J. Choyke, Phys. Rev. B **10**, 5091 (1974).

[4] A. Henry, C. Hallin, I. G. Ivanov, J. P. Bergman, O. Kordina, U. Lindefelt, and E. Janzén, Phys. Rev. B **53**, 13 503 (1996).

[5] R. P. Devaty and W. J. Choyke, Phys. Status Solidi A **162**, 5 (1997).

[6] A. Henry, O. Kordina, C. Hallin, C. Hemmingsson, and E. Janzén, Appl. Phys. Lett. **65**, 2457 (1994).

[7] I. G. Ivanov, C. Hallin, A. Henry, O. Kordina, and E. Janzén, J. Appl. Phys. **80**, 3504 (1996).

[8] L. L. Clemen, W. J. Choyke, R. P. Devaty, J. A. Powell, and H. S. Kong, in *Amorphous and Crystalline Silicon Carbide IV*, edited by C. Y. Yang, M. M. Rahman, and G. L. Harris, Springer Proceedings in Physics, Vol. 71 (Springer, Berlin, 1992), pp. 105–115.

[9] O. V. Kovalev in *Representations of the Crystallographic Space Groups*, edited by H. T. Stokes and D. M. Hatch (Gordon and Breach, New York, 1993).

[10] A. P. Cracknell, B. L. Davies, S. C. Miller, and W. F. Love, in *Kronecker Product Tables* (Plenum, New York, 1979), Vol. 1; A. P. Cracknell and B. L. Davies, *ibid.* Vol. 3.

[11] C. Persson and U. Lindefelt, J. Appl. Phys. **87**, 5496 (1997).

[12] The excitonic band gap corresponds to the energy of direct recombination of a free exciton, i.e., the forbidden zero-phonon free-exciton line should be observed at this energy position.

[13] J. R. Haynes, Phys. Rev. Lett. **4**, 361 (1960).

[14] W. Götz, A. Schöner, G. Pensl, W. Suttrop, W. J. Choyke, R. Stein, and S. Leibenzeder, J. Appl. Phys. **73**, 3332 (1993).

[15] P. J. Dean, J. R. Haynes, and W. F. Flood, Phys. Rev. **161**, 711 (1967).

[16] Bo Monemar (private communication).

[17] O. Kordina, A. Henry, J. P. Bergman, N. T. Son, W. M. Chen, C. Hallin, and E. Janzén, Appl. Phys. Lett. **66**, 1373 (1995). [See also W. J. Choyke, L. Patrick, and D. R. Hamilton, in *Proceedings of the International Conference on Semiconductor Physics, Paris, 1964*, edited by M. Hulin (Friedr. Vieweg & Sohn, Braunschweig, 1964), p. 751, where the same value for the excitonic band gap has been obtained by absorption measurements.]

[18] G. S. Mitchard and T. C. McGill, Phys. Rev. B **25**, 5351 (1982).

[19] D. W. Feldman, J. H. Parker, Jr., W. J. Choyke, and L. Patrick, Phys. Rev. **173**, 787 (1968).

[20] Unlike Raman-scattering experiments, neither the orientation nor the polarization of the exciting light influence the properties of the light emitted in luminescence. Nevertheless, it is convenient to use the same term ''backscattering configuration'' to underline the similarity of the experimental geometry for Raman and PL measurements.

[21] P. T. B. Schaffer, Appl. Opt. **10**, 1034 (1971).

[22] L. L. Clemen, R. P. Devaty, M. F. Macmillan, W. J. Choyke, A. A. Burk, Jr., D. L. Barrett, H. M. Hobgood, D. J. Larkin, and J. A. Powell, Inst. Phys. Conf. Ser. **137**, 147 (1994).

[23] J. Tersoff, Phys. Rev. B **39**, 5566 (1989).

[24] J. F. Cornwell, *Group Theory in Physics* (Academic, London, 1984), Vol. 1, Chap. 7.

[25] A. A. Maradudin, E. W. Montroll, G. H. Weiss, and I. P. Ipatova, *Theory of Lattice Dynamics in the Harmonic Approximation* (Academic, New York, 1971), Chap. VI.

[26] M. Hofmann, A. Zywietz, K. Karch, and F. Bechstedt, Phys. Rev. B **50**, 13 401 (1994).

[27] C. Persson and U. Lindefelt, Phys. Rev. B **54**, 10 257 (1996).

[28] G. F. Koster, J. O. Dimmock, R. G. Wheeler, and H. Statz, in *Properties of the Thirty-Two Point Groups* (MIT Press, Cambridge, MA, 1963).

[29] W. Heitler, The Quantum Theory of Radiation (Dover, New York, 1984).

[30] H. Berry Bebb and W. Williams, in *Transport and Optical Phenomena*, edited by R. K. Willardsson and A. C. Beer, Semiconductors and Semimetals Vol. 8 (Academic, New York, 1972), p. 181.

[31] L. Michel, M. B. Walker, and J. Zak, Phys. Rev. Lett. **74**, 4871 (1995).

[32] W. J. Choyke, R. P. Devaty, L. L. Clemen, M. F. MacMillan, M. Yoganathan, and G. Pensl, Inst. Phys. Conf. Ser. **142**, 257 (1996).

[33] L. Patrick, W. J. Choyke, and D. R. Hamilton, Phys. Rev. A **137**, A1515 (1965).